CHEMISTRY OF MATERIALS

pubs.acs.org/cm

Article

# Engineering Soft, Elastic, and Conductive Polymers for Stretchable Electronics Using Ionic Compatibilization

My Linh Le,[⊥] Intanon Lapkriengkri,[⊥] Kaitlin R. Albanese, Phong H. Nguyen, Cassidy Tran, Jacob R. Blankenship, Rachel A. Segalman,* Christopher M. Bates,* and Michael L. Chabinyc*

Cite This: *Chem. Mater.* 2023, 35, 7301−7310

Read Online

ACCESS | Metrics & More | Article Recommendations | Supporting Information

**ABSTRACT:** Designing materials that are soft, elastic, and conductive—a complement of properties that are useful in a number of applications such as bio-interfacing—remains a major challenge due to the high stiffness of conventional conductive materials. For all-polymer systems, this problem is compounded by the general immiscibility of elastomeric and conducting polymers, resulting in inhomogeneous mixing and poor properties. Here, electrostatic interactions are shown to be an effective strategy to compatibilize distinct polymer chemistries and backbone architectures, resulting in homogeneous and multifunctional polymer complexes that are soft, elastic, and highly conductive. An anionic conjugated polyelectrolyte (CPE) based on polythiophene was blended with a cationic bottlebrush polyelectrolyte (BPE). The CPE provided electrical conductivity, while the BPE helped to control the mechanical properties. Strong electrostatic attractions between oppositely charged side chains of the CPE and BPE suppressed phase separation and the polymers formed a nearly homogeneous charged complex despite marked differences in their chemistry and architecture. Upon drying of the solvent, the ionic groups act as dynamic crosslinks and the resulting material behaved as a viscoelastic and reprocessable solid. Once doped with a strong acid, this composite had an electrical conductivity of up to 0.3 S/cm while maintaining a low tensile modulus (0.2 MPa). These findings highlight the potential of designing advanced materials with processing and performance advantages through the use of electrostatic interactions to compatibilize polymers.

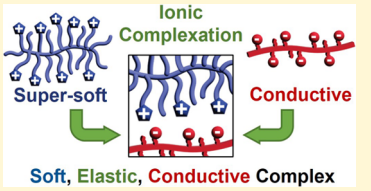




## INTRODUCTION

Applications such as soft robotics and wearable electronics create a need for materials with tailored electrical conductivity combined with mechanical properties that are in a challenging regime.[1,2] For example, the significant difference in mechanical modulus between conventional conductive materials ($E \geq 10^8$ Pa) and biological tissue ($E \leq 10^6$ Pa) leads to a severe interfacial mismatch in mechanical behavior.[3,4] Geometric engineering, i.e., utilizing spatial structuring of materials into meshes, kirigamis, or waves,[5−8] can be effective in imparting stretchability of intrinsically rigid conductive materials but is often challenging to implement. The development of materials that are both soft and electrically conductive would help address these issues.

Conjugated polymers offer the ability to form conductive materials with varying mechanical properties set by molecular design, but there are tradeoffs in their properties. The backbone of semiconducting polymers can be relatively stiff, but modifying the design of side-chains changes their mechanical softness. For example, polythiophenes with tetra(ethylene glycol) side-chains have been shown to have Young's modulus ($E$) of only 8 MPa around room temperature,[9] which is up to 2 orders of magnitude lower than polythiophenes with alkyl side-chains (60−900 MPa).[10−12] However, these softer conjugated polymers experience a significant increase in stiffness (up to 50 times) upon doping to achieve charge-carrier concentrations necessary for electrical conduction. Another strategy to reduce the stiffness of the backbone of semiconducting polymers is to add conjugation-break spacers.[13] This strategy also leads to tradeoffs between the electrical properties and the softness, with the modulus of these polymers falling within the 100−1000 MPa range.[13−17]

The formation of phase-separated blends or composites is another common strategy to achieve mechanical and electrical properties that are a combination of each individual material. For example, composites combining soft (e.g., PDMS-based silicone/triblock thermoplastic elastomers[18−20] or hydrogels[21,22]) and conductive materials [e.g., carbon nanotubes (CNTs),[23−25] metal,[26−29] or conjugated polymers[30−32]] allow tunable electrical and mechanical properties. CNTs have been successfully embedded in elastomers via solution mixing, melt mixing, and in-situ polymerization,[33] resulting in a wide range of properties—with conductivities $10^{-4}$−$10^0$ S/cm and elastic moduli $10^5$−$10^9$ Pa—that depends heavily on surface modification of the CNTs and the mixing procedure.[33−35] Similarly, blends of conductive polymers with elastomers can have electrical conductivity from $10^0$ up to $10^4$ S/cm with

Received: July 5, 2023
Revised: August 9, 2023
Published: August 29, 2023

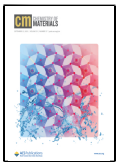

moduli ranging from $10^5$ to $10^9$ Pa.[30−32] This strategy has extensively examined for composites of PEDOT/PSS with elastomers or hydrogels to impart stretchability.[36] Soft composites ($E \leq 10^5$ Pa) have also been reported for systems using super-soft bottlebrush elastomers and CNTs[4,37] and alternatively hydrogels[21,22] with reported conductivities ranging from $10^{-3}$ to $10^1$ S/cm.[4,37,38] Given that these composites are physical blends, there are limitations to how their properties can be tuned.

In composites, the tradeoff between softness and conductivity originates from the need to form percolating transport pathways of the conductive material (that has a high stiffness). This ultimately increases the modulus of the composite and can render it unsuitable for soft electronics. While systems such as hydrogels possess low moduli that partially offset the stiffening effect from hard fillers, they rely critically on an exact degree of swelling or hydration which is impossible to maintain in many situations. Additionally, blending and homogenizing a soft, conductive composite is difficult because conductive particles have tendency to agglomerate, making them difficult to disperse homogeneously. The reaggregation of these particles during use results in poor stability and a deterioration in performance.[34] Moreover, blends of polymers are generally immiscible and tend to macrophase separate, which prevents the formation of a continuous transport pathway, causes undue brittleness, and presents significant processing complications. Lastly, the requirement of chemical crosslinking to impart elasticity in many systems introduces additional challenges such as poor crosslinker−polymer compatibility and curing procedures that compromise the stability of the blend.

Unlike the aforementioned approaches, ionic compatibilization provides the opportunity to effectively combine distinct polymers into a single homogeneous system. In mixtures of oppositely charged ionic polymers, strong electrostatic attraction between the two species limits the domain size of microphase separation and the long-range nature of these interactions can even overcome the enthalpic penalty that leads to macrophase separation.[39−47] Mean-field models suggest the inclusion of just 10 charges per polymer chain increases the critical segregation strength $(\chi N)_c$ of a blend from 2 to 400 in the typical dielectric environment of a polymer melt.[48] We have previously investigated the processability, self-assembly, photophysical, and optoelectronic properties of complexes obtained by blending linear ionic conjugated polymer and linear polyelectrolytes.[49−51] However, the impact of molecular architecture in these complexes has not been investigated nor the ability to leverage ion compatibilization in formulating multifunctional complexes.

Here, we find that ionic interactions effectively stabilize a homogeneous blend of two polymers that differ not only in chemistry (i.e. semiconducting vs insulating) but also in architecture, resulting in exceptionally soft and conductive polymer complexes from a linear conjugated polymer (CPE) and a bottlebrush polyelectrolyte (BPE). These solid-state CPE−BPE complexes form ionically crosslinked polymer networks having appreciable elasticity without any added crosslinker and can be (re)processed by simple molding at room temperature. The CPE, despite being highly dispersed in the complex, forms a percolating conduct network. As a result, the conductivity of CPE−BPE complexes is 0.3 S $cm^{-1}$ after doping with a strong acid. Doping also decreases the modulus of the complex from 0.7 to 0.2 MPa. The complex (both pristine and doped) can be stretched to appreciable strains (450 and 100%, respectively) followed by substantial elastic recovery. These findings highlight the potential of using electrostatic interactions to create multifunctional polymer blends with processing and performance advantages.

## RESULTS AND DISCUSSION

To target soft and conducive composites, coacervates were formed from an anionic conjugated polyelectrolyte (CPE) and a cationic BPE (Figure 1a with synthetic details in the

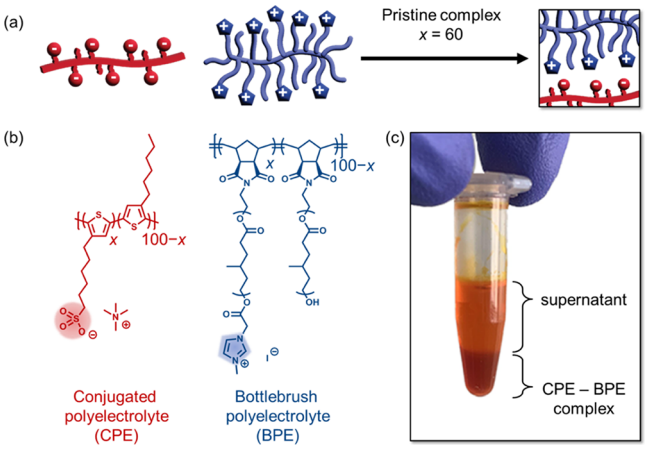


**Figure 1.** (a, b) Coacervation of a conjugated polyelectrolyte (CPE, red) and bottlebrush polyelectrolyte (BPE, blue), each with 60% charge fraction ($x$ = 60), leads to an ionically crosslinked polymer complex. (c) Photograph of phase separation upon mixing CPE and BPE solutions, producing a concentrated coacervate (darker orange, bottom) in coexistence with polymer-deficient supernatant (lighter orange, top).

Supporting Information and Figures S1−S10). For the bottlebrush component, poly(4-methyl caprolactone) (PMCL) was selected as the side-chain structure because of its (i) low glass-transition temperature ($T_g$ = −60 °C),[52] (ii) lack of crystallinity, and (iii) hydroxyl chain ends that facilitate post-polymerization modification to install pendant ions. Bottlebrush precursors (before functionalization with ions) were synthesized via grafting-through polymerization using ring-opening metathesis polymerization (ROMP) as described in the literature.[52] For all samples discussed herein, the norbornene-functionalized PMCL macromonomer degree of polymerization ($N_{SC}$ = 17) was set below the entanglement molecular weight.[52] After polymerizing the macromonomer via ROMP to a backbone degree of polymerization ($N_{BB}$) around 100, the resulting bottlebrush polymer was functionalized with cationic imidazolium chain ends having iodide counterions via carbodiimide coupling and $S_N2$ chemistry. Complete synthetic details are provided in the Supporting Information. Importantly, the wide electrochemical stability window of imidazolium[53] allows it to remain stable upon electrical doping of the semiconducting polymer after blending. As evidenced by $^1$H nuclear magnetic resonance spectroscopy, this sequence of post-polymerization modification reactions yielded a single imidazolium unit attached to 60% ($x$) of side-chains. Notably, ionic functionalization did not result in a significant increase in $T_g$ for the bottlebrush polymer, which remained around $T_g$ = −55 °C (Figure S11). To form an ion complex, this charged bottlebrush polymer was complexed with an anionic semi-


https://doi.org/10.1021/acs.chemmater.3c01685
Chem. Mater. 2023, 35, 7301−7310

conducting polymer, poly[6-(thiophen-3-yl)hexane-1-sulfonate, which has good electronic properties in complexes with linear polyelectrolytes.[51] The fraction of charged repeat units on the CPE was tailored to match the value per bottlebrush molecule (60%). After mixing and removal of the solvent (water) by drying in vacuo, the coacervate transformed into an elastic solid containing ionic crosslinks.

Despite a pronounced difference in chemistry and architecture, the CPE and BPE are effectively compatibilized by electrostatic interactions. The CPE−BPE coacervate ($x$ = 60%) appears to be well-mixed on the micrometer scale by optical microscopy unlike a control sample of analogous uncharged polymers ($x$ = 0%) that shows significant phase separation and aggregation of the conjugated polymer (Figure 2). Although the charge fraction with respect to the repeating

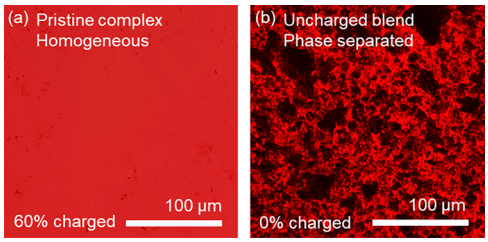


**Figure 2.** Optical micrographs of (a) solid-state complex obtained after drying a blend of the CPE and BPE with $x$ = 60% charge. The uniform red color indicates a homogeneous distribution of the CPE in the blend on the micrometer length scale that is consistent with phase compatibility between CPE and BPE. (b) In contrast, a blend of uncharged poly(3-hexylthiophene) (P3HT) and bottlebrush ($x$ = 0%) undergoes macroscopic phase separation.

unit of the main chain of both polymers is around 60%, the charge density of the BPE is much lower because the long side-chains—with, on average, $N_{SC}$ = 17 repeat units per side-chain—act as a diluent. Consequently, there is only 1 cation−anion pair per 18 monomeric units in the BPE. The observation of homogeneous mixing is consistent with mean-field calculations that predict only a few charges per polymer chain are needed to completely compatibilized most polymers.[48] We also note that while ionic interactions have been successfully used to stabilize mixtures of two linear polymers,[49−51] less effort has been invested in studying different architectures like the BPE reported here. Clearly, electrostatic interactions are a powerful tool for mixing different types of polymer architectures as well.

We determined the composition of the resulting solid-state complex derived from drying of the coacervate blend using X-ray photoelectron spectroscopy (XPS). If the stoichiometry of the CPE−BPE complex was 1:1 on a per-molecule basis, the N/S ratio in XPS would lie between 1.4:1 and 1.75:1 depending on the number of residual tetramethylammonium ions remaining after coacervation; this estimate takes into account the total amount of nitrogen—from both tetramethylammonium cations and the imidazolium/imides in BPE—relative to sulfur which is only found in CPE along the thiophene backbone and in the sulfonate groups. In contrast, by XPS, the measured ratio of nitrogen to sulfur is N/S ≈ 2:1. This excess of nitrogen relative to expectations suggests that the molar ratio of BPE to CPE repeat units is between 1.2 and 1.5. The BPE therefore preferentially partitions into the complex coacervate phase while the CPE preferentially partitions into the supernatant, a situation that is common in the formation of coacervates from linear polymers with a mismatch in charge density.[54] Although the inferred ratio of repeat units with respect to the main polymer chain is close to unity, it is important to appreciate that the complex is still mainly composed of BPE molecules due to their much larger size; the molar mass of a CPE repeat unit is 213.4 g/mol, while that of a single side-chain in BPE is approximately 12 times larger (2478 g/mol: the sum of 17 side-chain repeat units on average). As a result, the BPE constitutes approximately 93−95 vol % (95−96 wt %) of the complex with conductive CPE the small remainder (details of this calculation are discussed in the Supporting Information).

While the BPE−CPE complex is homogeneously mixed at micrometer length scales, a hierarchical local structure is present within the material. As shown in Figure 3a, small-angle

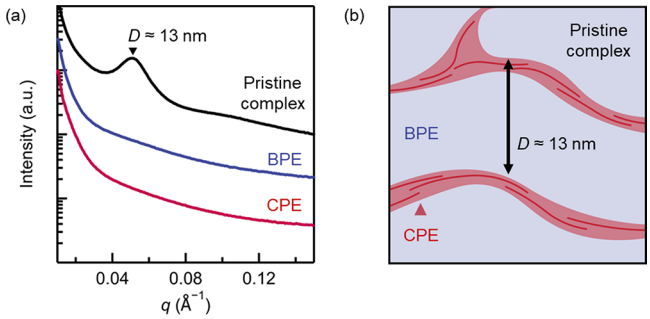


**Figure 3.** (a) SAXS patterns of the neat CPE, neat BPE, and the undoped CPE−BPE complex; a peak at a length scale of ≈13 nm indicates the formation of nanostructure in the complex. (b) Proposed nanostructure of the pristine complex with domains of semiconducting CPE (red) and the BPE (blue).

X-ray scattering (SAXS) of the pristine complex contains a broad peak centered at $q \approx 0.05$ Å$^{-1}$ corresponding to a correlation length of 13 nm. Because the SAXS profile of each component individually is featureless, this correlation length indicates that nanoscopic structure arises as a result of complexation. Interestingly, the length scale is very close to the estimated size of a single pair of BPE and CPE molecules (see Figure S12 and associated discussion). Because the CPE is only present in a minor quantity within the complex (<5 vol % as described above), we postulate that the pristine complex takes on a morphology as illustrated in Figure 3b. Charge-mediated complexation should occur at the BPE−CPE interface because the low-dielectric-constant environment requires close contact between oppositely charged ions. As the BPE is present in excess, these majority domains likely contain more than one bottlebrush molecule and cations buried within the interior that are charge-compensated by iodide counterions. Although XPS spectra do not show the presence of iodine since it is present in such small concentrations (i.e. ≈0.3 atom% in neat BPE), we were able to confirm its presence after complexation with dynamic secondary-ion mass spectrometry (Figure S13). Our electrical data (vide infra) suggest that the CPE chains form a thin percolating network in a matrix of BPE.

Due to the significant dilution of the CPE, no scattering signature was observed at smaller length scales for it in the complex, unlike the relevant length scales associated with the BPE that remain unchanged upon complexation. As shown in Figure S15, a peak at $q \approx 0.4$ Å$^{-1}$ ($d$ = 1.6 nm) in wide-angle X-ray scattering (WAXS) in both the BPE and the ion complex


https://doi.org/10.1021/acs.chemmater.3c01685
Chem. Mater. 2023, 35, 7301−7310

likely corresponds to side-chain correlations along the BPE backbone.[55] In contrast, the neat CPE forms a semicrystalline solid with chains stacked along both the backbone and side-chain directions; Bragg reflections at $q \approx 0.27$, 0.55, and 1.67 Å$^{-1}$ that corresponds to the (100), (200) (alkyl stacking), and (010) ($\pi$-stacking) of CPE crystallites are in agreement with studies of thin films in the literature.[56] Such crystallinity is absent in our prior work on linear coacervate blends,[51] where a similar semiconducting poly(thiophene) with $x$ = 60% and $M_n$ = 8 kDa was amorphous, a difference that we attribute to the higher molecular weights used herein, $M_n$ = 11 and 16 kDa. None of these WAXS features show up in after complexation indicating the absence of crystallites of the CPE in the complex.

Photoluminescence (PL) spectroscopy indicates a stronger J-type characteristic of CPE aggregates in the complex compared to its neat form and an improvement in intrachain structural order upon complexation. As shown in Figure 4, the

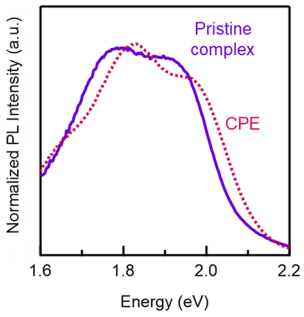


**Figure 4.** Normalized photoluminescence spectra of the pristine CPE−BPE complex and a film of the neat CPE.

PL spectrum of the complex exhibits a higher $I_{0-0}/I_{0-1}$ ratio (0.94) compared to the neat CPE (0.82). In the limit of pure H-type (inter-chain) aggregates, the 0−0 transmission is dipole-forbidden. As a result, the more intense 0−0 peak in the complex PL spectrum indicates that the electronic coupling of CPE chains in the complex has more J-type character than in the neat CPE. As the CPE disperses within the BPE matrix at 5 vol %, chains intuitively become more isolated from each other. Furthermore, the complex also has a lower $I_{0-2}/I_{0-1}$ ratio (0.37) compared to the neat CPE (0.48). The intensity of the 0−2 emission peak has been shown to be an effective measure of intrachain conjugation,[57] with longer intrachain conjugation lengths yielding weaker 0−2 emission. As a result, the smaller $I_{0-2}/I_{0-1}$ ratio of the complex suggests that complexation with the BPE enhances exciton delocalization along the CPE backbone. This observation differs from our previous result with linear polyelectrolytes where complexation-induced planarization of the CPE occurs only in complexes of highly charged polymers.[51] We hypothesize that the cause for this different behavior of the CPE−BPE complex is asymmetry of this system in both the volume fraction of each polymer and their relative molecular sizes.

Doping of the complex was carried out to yield electrically conductive films. Films of the CPE−BPE complex were exposed to bistriflimidic acid (HTFSI) vapor at 55 °C for 1 h, followed by heating for 24 h in an enclosed chamber to ensure sufficient diffusion of dopant molecules into the material. HTFSI was chosen as the dopant because it sublimes at room temperature, so no excessive heating was required. This protocol is known to be effective for doping semiconducting polymers in linear coacervates via diffusion into ionically crosslinked polymer complexes.[49,51] Doping was stopped after no further increase in electrical conductivity was observed. Effective doping was confirmed by monitoring the UV−vis spectrum and observing bleaching of the neutral CPE backbone absorption with the emergence of a polaronic absorption peak at ≈ 1.7 eV and bipolaron absorption at $h\nu <$ 1.5 eV (Figure S16).

As expected, the doped complex is electronically conductive indicating that the CPE chains can form a macroscopically connected network throughout the complexed material. The conductivity of HTFSI-doped complexes varies significantly from $3 \times 10^{-3}$ to $3 \times 10^{-1}$ S/cm. Of note, complexes had better conductivities ($5 \times 10^{-2}$−$3 \times 10^{-1}$ S/cm) when synthesized from CPE with larger molecular weights (16 kDa) compared to smaller ones (11 kDa, $3 \times 10^{-3}$−$2 \times 10^{-2}$ S/cm) (Table S2). There may also be a pronounced contribution from processing, for example during hot pressing and vapor doping, neither of which are particularly well-controlled. Despite this variation, the conductivity of complexes when normalized by the CPE concentration (of order 5% by volume) is significantly higher than measured for neat CPE thin films ($6 \times 10^{-3}$ S/cm); for example, the conductivity of the most conductive complex sample ($3 \times 10^{-1}$ S/cm) after normalization for the estimated volume fraction is 4−6 S/cm—within the range typically reported for doped poly(3-hexylthiophene), P3HT, films. This result is remarkable as it indicates complexation with an insulating bottlebrush polymer maintains the charge-carrier mobility of the semiconducting polymer. One possible explanation is the planarization of the CPE backbone, consistent with Figure 4, leading to efficient intrachain transport and interconnectivity of the conjugated chains. This inference is further supported when considering the percolation threshold reported for conductor−insulator blends. Specifically, for various blends of conductive and insulating polymers, a commonly observed percolation threshold for the insulator−metal transition is 16 vol %,[58,59] which is near the expected threshold for a dispersion of spherical particles in three dimensions.[60] However, the value decreases rapidly as the conductive component forms domains with more elongated and/or lower dimensional shapes with improved alignment. For example, the percolation threshold can be as low as 0.05 vol % for pancakes of conducting polymers that are templated onto a mechanically connected gel network.[61] In our system, the complex is conductive with approximately 5−7 vol % of the conducting component, suggesting the percolation threshold for this electrostatically complexed blend is below 5 vol %. These results support a previously proposed design rule for lowering the percolation threshold in conducting−insulating polymer blends by dispersing the conductive component at the molecular level instead of forming larger conducting aggregates inside an insulator matrix.[62]

Despite the lack of entanglements in the bottlebrush portion of these complexes, the CPE−BPE complexes are elastic because their ionic interactions cause crosslinking. As shown in Figure 5, the complexation of BPE with CPE yields a viscoelastic solid with the shear storage modulus $G'$ larger than the loss modulus $G''$ across a broad range of frequencies. Notably, the plateau modulus of the pristine complex remains quite soft ($G'_{pristine} \approx 0.14$ MPa), which is similar to non-ionic bottlebrush elastomers[63,64] as well as soft tissue; a detailed


https://doi.org/10.1021/acs.chemmater.3c01685
Chem. Mater. 2023, 35, 7301−7310

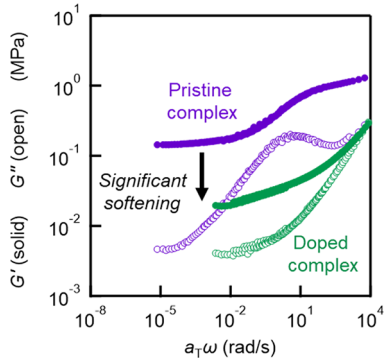


**Figure 5.** Rheological master curves of CPE−BPE ion complexes before (pristine) and after doping with HTFSI where the closed and open symbols represent G′(storage) and G″(loss) components respectively. The addition of the dopant leads to a significant reduction in both components of the modulus.

comparison of these and other materials is provided in Figure S22.

As shown in Figure 5, doping decreases the shear modulus by roughly fivefold ($G'_{complex} \approx 0.03$ MPa) while retaining solid-like character ($G' \gg G''$ across all frequencies). Figure 6

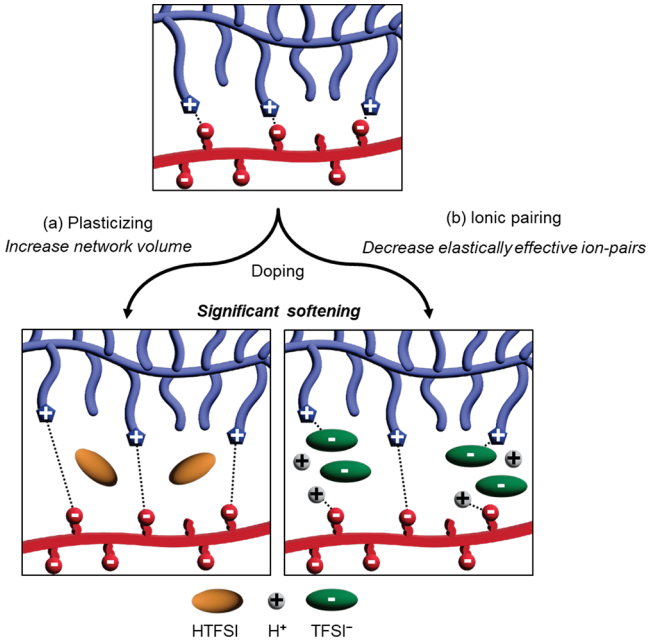


**Figure 6.** Schematic of the impact of doping by HTFSI on the mechanical properties of the CPE−BPE. The additional ions introduced by doping (a) can increase the network volume and potentially plasticize the blend and (b) can decrease the number of effective crosslinks between the two polymers.

outlines two potential sources of the decrease in plateau modulus that are consistent with the basic theory of rubber elasticity (eq 1):

$$G = k_b T \frac{n}{V} \quad (1)$$

where $G$ is the shear modulus, $k_b$ is Boltzmann's constant, $T$ is absolute temperature, $n$ is the number of effective elastic crosslinks, and $V$ is the network volume.[65] Plasticization by the introduction of HTFSI (Figure 6a),[66] even without significant proton transfer, would increase the network volume and dilute crosslink density, in analogy to swollen systems, leading to a decrease in $G$. However, the 20% increase in mass observed upon doping is inconsistent with the estimated 80 wt % of HTFSI needed to decrease $G'$ by a factor of five based only on plasticization (see the Supporting Information). A second plausible mechanism to explain the pronounced softening upon doping is the formation of elastically ineffective ion pairs (Figure 6b). After proton transfer, the ionization of HTFSI into $H^+$ and $TFSI^-$ could break the initial ionic crosslinks, leading to a decrease in the number of effective crosslinks. Other changes including electronic doping of the CPE backbone and protonation of hydroxyl chain ends along the bottlebrush ($pK_a \approx 15$) (Figure S24) may also contribute to softening in a nontrivial way.[67,68]

The CPE−BPE complexes are soft, deformable, and elastic both before and after doping as measured in uniaxial tension. As shown in Figure 7a, the pristine complex exhibits an initial linear elastic region up to 20% strain characterized by a low elastic modulus $E \approx 0.7$ MPa that is order of magnitude smaller than typical semicrystalline conducting polymers (≈10−1000 MPa).[9] For the doped complex, the elastic region is extended to nearly 45% strain with a significant decrease in $E$

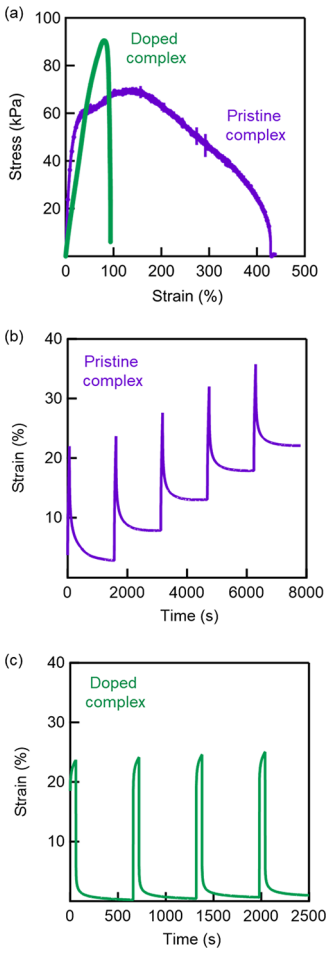


**Figure 7.** Uniaxial tensile measurements of free-standing dog-bone structures of CPE−BPE complexes before and after doping. (a) Single extension measurements of the samples until failure. Cyclic stress-controlled recovery measurements of the (b) pristine complex and (c) doped complex when subjected to 20% elongation over 1 min and subsequent relaxation upon removal of the applied stress.


https://doi.org/10.1021/acs.chemmater.3c01685
Chem. Mater. 2023, 35, 7301−7310

≈ 0.2 MPa. The wider range of strain corresponding to elasticity in the doped complex is likely caused by the plasticization and partitioning of HTFSI as discussed above. At larger strains, both the pristine and the doped complexes can be extended to appreciable elongation before break (pristine = 430%, doped = 94%). This stretchability is higher than many previously reported conjugated-polymer−linear elastomer composites that often fail at <150% strain.[19,69,70]

The complex shows the appreciable recovery of mechanical and transport properties after deformation. In particular, cyclic experiments were carried out during with a 25 kPa stress applied for 1 min, resulting in a ∼20% elongation, followed by release and a relaxation period that lasted until no further change over time was observed (Figure 7b). The pristine complex showed 87% recovery after the first cycle and its recovery remained consistently >75% after subsequent cycles with notable plastic deformation. In contrast, the doped complex consistently showed higher recoveries, circa 99%, over multiple cycles and essentially no plastic deformation. To complement these mechanical measurements, we measured the sheet resistance of the doped complex as a function of applied strain by supporting it on a polystyrene-*block*-polyethylene/polybutylene-*block*-polystyrene substrate (SEBS, Kraton G1652M) (Figure S23a). In this geometry, the substrate was clamped directly instead of the complex to avoid compression and shearing effects that could obfuscate the interpretation of resistance measurements. Figure 8 compares the change in resistance upon deformation to a model of an ideal elastomeric conductor with an unchanging bulk resistivity (details of the calculation are provided in the Supporting Information). The increase in resistance of the doped complex when subjected to strain deviates from the behavior expected for an ideal elastomeric conductor with a smaller change in resistance with extension. This deviation could be due to changes in the alignment of the CPE chains that decrease the resistivity $\rho$ of the complex. Second, the ideal elastomer model assumes an isotropic material with a Poisson's ratio of 0.5 whereas the doped complex here likely deviates from this value. Furthermore, after deforming the sample and compressing it back to 0% strain, the recovery of the initial resistance over 1 day suggests further (sluggish) rearrangement within the sample.

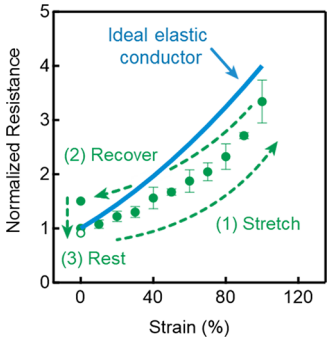


**Figure 8.** Normalized resistance of a film of the doped complex supported by a SEBS layer (relative to 0% strain) as a function of applied strain. The solid line shows a prediction for an ideal elastic conductor with a conductivity that is independent of strain. The open symbol shows the recovery of the resistance after deformation, compression, and one day of rest.

## CONCLUSIONS

Ion complexation between two oppositely charged polyelectrolytes is an effective strategy to engineer stretchable, elastic, and semiconducting materials. Mixing an anionic semiconducting polymer and cationic bottlebrush resulted in macroscopically homogeneous coacervates with nanostructuring derived from ion complexation. After drying, these materials are soft ($E \approx 0.2-0.7$ MPa), stretchable, and electrically conductive (up to $3 \times 10^{-1}$ S/cm) when doped with strong acid. This simple design strategy requires no additional crosslinkers or complex processing optimization to create a synergistic combination of elasticity and conductivity. The use of bottlebrush polymers in complexes allows further control through their molecular architecture that we have not explored here. For example, the bottlebrush side-chains can be modified, e.g., the degree of polymerization and the grafting density, to further tune their properties. We have also only examined one particular charge density on the CPE and bottlebrush polymer with the question remaining of how to further control electrostatic crosslinking and structural relaxations. In summary, this work underscores the potential of using ionic compatibilization to engineer multifunctional polymeric materials with implications for applications such as next-generation electronics and bio-interfacing.

## EXPERIMENTAL SECTION

**Materials.** *N*-(hydroxyethyl)-*cis*-5-norbornene-*exo*-2,3-dicarboximide was prepared according to the literature.[71] Grubbs' second-generation metathesis catalyst [$(H_2IMes)(PCy_3)(Cl)_2Ru$ = CHPh] was purchased from Sigma Aldrich. Grubbs' third-generation metathesis catalyst [$(H_2IMes)(pyr)_2(Cl)_2Ru$ = CHPh] (G3) was prepared according to the literature.[72] *N*-(hydroxyethyl)-*cis*-5-norbornene-*exo*-2,3-dicarboximide (Nb-OH) was synthesized according to the literature.[71] Poly(4-methylcaprolactone) (PMCL) macromonomer and bottlebrushes were prepared using previously reported methods.[73] Tin(II) 2-ethylhexanoate ($Sn(Oct)_2$, Sigma Aldrich, 92.5−100%) was purified according to the literature.[74] 2,5-dibromo-3-(6-bromohexyl)thiophene (eNovation Chemicals LLC), 1*H*-Imidazol-1-ylacetic acid (Sigma Aldrich). *N*-(3-Dimethylaminopropyl)-*N*′-ethylcarbodiimide hydrochloride (EDC·HCl, Sigma Aldrich, commercial grade), 4-(Dimethylamino)pyridine (DMAP, Sigma Aldrich), ethanol amine (Sigma Aldrich, purity ≥99%), Chloroform (Sigma Aldrich, anhydrous, contains amylenes as a stabilizer, purity ≥99%), acetone (Fisher Scientific, purity ≥99.5%), methanol (Fisher Scientific, purity = 99.5%), dichloromethane (Fisher Scientific, purity ≥99.5%), ethyl vinyl ether (ACROS Organic, Contains 0.1% KOH as stabilizer, purity = 99%), dimethylformamide (dry over molecular sieve), $CDCl_3$ (Cambridge Isotope Laboratories, purity = 99.8%), and acetone-$d_6$ (Cambridge Isotope Laboratories, purity = 99.9%) were used as received.

**Sample Preparation.** *Complex Formation.* 120 mM stock solutions of the BPE and the CPE were prepared by dissolving the polymers in adequate amount of solvent mixtures of 80%THF:20% water and 60%THF:40% water, respectively. BPE and CPE solutions were mixed in the stoichiometric ratio in an Eppendorf tube, and the mixture was vortexed for 1 min to ensure even mixing. The coacervate droplets that formed during the complexation process were collected by centrifugation of the tube at 7000 rpm for 10 min followed by decanting the supernatant. The bulk complex sample was obtained by drying the coacervate at 50 °C under house vacuum overnight, followed by 24 h of mild heating at 50 °C under high vacuum (≈$2 \times 10^{-8}$ Torr).

*Film Fabrication.* The complex film was obtained by drop casting the CPE−BPE coacervate onto a silicon substrate with custom-made gold digits, and the substrate was heated at 50 °C for 10 min to remove most solvent. The substrate with the roughly dried complex


https://doi.org/10.1021/acs.chemmater.3c01685
Chem. Mater. 2023, 35, 7301−7310

was then pressed between 2 metal plates separated by Teflon spacers, resulting in a ≈ 20−30 μm thick film. The film was then fully dried under high vacuum (≈2 × $10^{-8}$ Torr) at 50 °C overnight. CPE films were obtained by spin casting the 120 mM stock solution onto the substrate at 500 rpm for 2 min 30 s. For XPS and dynamic secondary ion mass spectroscopy (DSIMS) experiments, complex films were obtained by smearing a small fraction of dry the bulk sample onto silicon substrates using a single-edge razor blade.

*Vapor Doping.* Electrical doping of the CPE−BPE complex was done inside a nitrogen glovebox. The complex film on the substrate was attached to a lid of a glass jar with HTFSI crystals. The jar was closed tightly and heated at 50 °C on a hot plate for 13 min (CPE) or 1 h (CPC). For the complex film, the film was transferred to another closed clean glass jar and kept at 55 °C for an additional 48 h to promote efficient diffusion of dopants into the film and to prevent leakage of dopant vapor. After this, the film was put under vacuum for 2 days to fully remove all the excess HTFSI molecules. For bulk samples, vapor doping was carried out for 48 h, as we observed that after this no further mass gain was observed. The sample was then put under vacuum for an additional 72 h to obtain the doped bulk sample.

**Materials Characterization.** *Nuclear Magnetic Resonance (NMR).* All bottlebrush polymer $^{1}$H NMR spectra were collected using a Varian Unity Inova AS600 600 MHz equipped with a 5 mm Varian triple resonance $^{1}$H/$^{13}$C/$^{15}$N inverse detection probe with *z*-axis pulsed field gradient (PFG). All linear polymer $^{1}$H NMR spectra were collected using a 600 MHz SB Varian VNMRS equipped with a double resonance Broadband Probe Head 600 DB Auto X. Small molecule $^{1}$H and $^{13}$C NMR were collected using a *Bruker Avance NEO 500 MHz* equipped with a CryoProbe Prodigy BBO probe with *z*-axis PFG.

*Size-Exclusion Chromatography (SEC).* SEC was performed on a Waters Alliance HPLC System equipped with a 2690 Separation Module, or a Waters Alliance HPLC system with an Agilent PLgel 5 μm MiniMIX-D column. The former uses chloroform with 0.25% triethylamine, while the latter uses THF as the eluent. For the former, the refractive index from a Waters 2410 Differential Refractometer detector was used to estimate the molar mass and dispersity relative to linear polystyrene standards. For the latter, refractive index traces from a Waters 2414 detector were used for molecular weight determination using polystyrene calibration standards (Agilent Technologies).

*Tensile Tests.* Uniaxial tensile testing was performed with a TA.XTplusC texture analyzer equipped with A/MTG tensile grips. Samples were clamped without additional adhesive. The pristine complex was prepared by simple pressing into a metal rectangular mold (8 mm wide × 15 mm long × 0.5 mm thick) sandwich between two PTFE sheets at room temperature using 1 metric ton of force. The samples were punched into a dog-bone shape (10 mm long × 1.5 mm wide × 0.5 mm thick) using a brass punch. The doped complex was prepared by first simple pressing of CPE−BPE into a rectangular shape previously described, then the rectangular-shaped sample was doped with HTFSI as described in the Vapor Doping section. All measurements were done at a constant strain rate of 1 $min^{-1}$.

*Dynamic Mechanical Analysis.* Cyclic stress-controlled recovery measurements were performed on a Discovery DMA 850 at room temperature. A film clamp was used, and the sample was clamped without additional adhesive. In each measurement, the sample was strained with a constant stress (dwell time = 1 min) before letting it to relax. The samples were prepared similarly to the uniaxial tensile measurements.

*Rheology.* A strain-controlled ARES-G2 rheometer equipped with a liquid nitrogen dewar from TA Instruments was used to investigate the shear stress relaxation and linear viscoelastic properties of the blend. A pair of 8-mm stainless steel parallel plates were used for all measurements. Strain-sweep experiments were performed prior to measurement to determine the linear-viscoelastic region (LVE) of the materials. Stress relaxation data were collected under a small amount of axial force to prevent slipping. To generate master curves, isothermal frequency sweep between 100 and 0.1 rad/s at a constant 1% strain was collected at different temperatures. A master curve was constructed using time−temperature superposition (TTS) under Williams−Landel−Ferry (WLF) relation.

*Differential Scanning Calorimetry (DSC).* DSC measurements were performed on a DSC 2500 calorimeter (TA Instruments). Approximately 5 mg of material was sealed in Tzero hermetic pans (TA Instruments) and cycled between −80 and 200 °C at 10 °C/min. The glass transition temperature ($T_g$) of the sample was determined on the second heating cycle using the midpoint analysis method.

*Optical Spectroscopy.* UV−vis absorption spectra of CPE and the complex films were taken using an Agilent Cary 60 UV−vis spectrophotometer. All measurements were done at ambient temperature (≈ 25 °C). Emission spectra were taken using a Horiba FluoroMax 4 spectrometer at 450 nm excitation wavelength with a 495 nm long pass filter. The sample is illuminated by a 150 W xenon, continuous output, ozone-free lamp. The emission spectrum of each film was averaged over 3 scans.

*Conductivity Measurements.* The in-plane electronic conductivity of the samples was measured with transmission line measurements using custom made gold digits on silicon substrates. For the strain-dependent and strain cycling conductivity tests, the complex film was casted onto a Kraton substrate. The Kraton substrate and the supported complex film weresubjected to the designated strain. For the cycling test, the sample was first subjected to 20% strain for 15 s, and the measurement at 0% strain was done after the sample was let to relax for 15 min. All measurements were done with a Keithley 6485 picoammeter and were carried out inside a nitrogen glovebox at room temperature.

*X-ray Photoelectron Spectroscopy.* The XPS analyses were performed using a ThermoFisher Escalab Xi+ with Al K$\alpha$ X-ray radiation, in conjunction with an electron flood gun. We quantified the relative atomic percentages from XPS survey spectra through the Avantage software suite, provided by Thermo Fisher Scientific Inc. We specifically focused on integrating and normalizing the C 1s (CPE and BPE), N 1s (BPE and CPE counterion), O 1s (BPE, CPE counterion, and substrate), S 2s (CPE and CPE counterion), and Si 2p (substrate) peaks by their respective photoionization cross sections. The iodine signal, which was at a comparable level to noise in the survey spectra, was omitted from our analysis.

*Dynamic Secondary Ion Mass Spectroscopy.* For the DSIMS analysis, films were first coated with a thin layer of Pd/Au to augment conductivity. Examinations were then carried out using a Cmaeca IMS 7f Auto SIMS. Following this, the films were sputtered with reactive $O_2^+$ ions over an area of 63 × 63 $\mu m^2$, while simultaneously monitoring the counts per second of $^{127}$I within the central 50 × 50 $\mu m^2$ region, against sputtering time. In two distinct regions, a considerable and nearly consistent level of $^{127}$I signal was detected throughout the sputtering depth of the sample (refer to Figure S2). We attribute this to the retention of I- ions within the BPE-rich domains.

## ■ ASSOCIATED CONTENT

### Supporting Information

The Supporting Information is available free of charge at https://pubs.acs.org/doi/10.1021/acs.chemmater.3c01685.

Synthetic procedures; materials characterization data ($^{1}$H NMR and SEC); X-ray scattering; UV−vis spectra; rheological master curves; stress−strain and mechanical relaxation data; and data on electrical conductivity as a function of strain (PDF)

## ■ AUTHOR INFORMATION

### Corresponding Authors

**Rachel A. Segalman** − *Materials Department, Department of Chemical Engineering, and Materials Research Laboratory, University of California, Santa Barbara, California 93106, United States;* orcid.org/0000-0002-4292-5103; Email: segalman@ucsb.edu



https://doi.org/10.1021/acs.chemmater.3c01685
*Chem. Mater.* 2023, 35, 7301−7310

**Christopher M. Bates** − *Materials Department and Materials Research Laboratory, University of California, Santa Barbara, California 93106, United States;* orcid.org/0000-0002-1598-794X; Email: cbates@ucsb.edu

**Michael L. Chabinyc** − *Materials Department and Materials Research Laboratory, University of California, Santa Barbara, California 93106, United States;* orcid.org/0000-0003-4641-3508; Email: mchabinyc@engineering.ucsb.edu

### Authors

**My Linh Le** − *Materials Department, University of California, Santa Barbara, California 93106, United States;* orcid.org/0000-0003-2385-0385

**Intanon Lapkriengkri** − *Materials Department, University of California, Santa Barbara, California 93106, United States*

**Kaitlin R. Albanese** − *Department of Chemistry & Biochemistry and Materials Research Laboratory, University of California, Santa Barbara, California 93106, United States;* orcid.org/0000-0003-1129-8052

**Phong H. Nguyen** − *Department of Chemical Engineering, University of California, Santa Barbara, California 93106, United States*

**Cassidy Tran** − *Materials Research Laboratory, University of California, Santa Barbara, California 93106, United States*

**Jacob R. Blankenship** − *Department of Chemistry & Biochemistry and Materials Research Laboratory, University of California, Santa Barbara, California 93106, United States*

Complete contact information is available at: https://pubs.acs.org/10.1021/acs.chemmater.3c01685

### Author Contributions

⊥M.L.L. and I.L. contributed equally to this work.

### Notes

The authors declare no competing financial interest.

## ■ ACKNOWLEDGMENTS

This work was funded by the Department of Energy Office of Basic Energy Sciences under Grant No. DE-SC0016390 (characterization) and the National Science Foundation under Award No. CMMI-2053760 (synthesis). C.M.B. thanks The Camille and Henry Dreyfus Foundation for partial support. The authors acknowledge the use of shared facilities of the UCSB MRSEC (NSF DMR 1720256), a member of the Materials Research Facilities Network (www.mrfn.org). Tensile testing and X-ray scattering experiments were supported by the BioPACIFIC Materials Innovation Platform of the National Science Foundation under Award No. DMR-1933487. This research used resources of the National Synchrotron Light Source II, a U.S. Department of Energy Office of Science User Facility (DE-SC0012704; beamline 11-BM). I.L. is grateful for DPST fellowship from the Institute for the Promotion of Teaching Science and Technology, Thailand. We thank beamline scientist Dr. Ruipeng Li for helping with the collection of X-ray scattering data.

## ■ REFERENCES

(1) Kang, J.; Son, D.; Vardoulis, O.; Mun, J.; Matsuhisa, N.; Kim, Y.; Kim, J.; Tok, J. B.-H.; Bao, Z. Modular and Reconfigurable Stretchable Electronic Systems. *Adv. Mater. Technol.* **2019**, *4*, No. 1800417.

(2) Wallin, T. J.; Pikul, J.; Shepherd, R. F. 3D Printing of Soft Robotic Systems. *Nat. Rev. Mater.* **2018**, *3*, 84−100.

(3) Rus, D.; Tolley, M. T. Design, Fabrication and Control of Soft Robots. *Nature* **2015**, *521*, 467−475.

(4) Xu, P.; Wang, S.; Lin, A.; Min, H.-K.; Zhou, Z.; Dou, W.; Sun, Y.; Huang, X.; Tran, H.; Liu, X. Conductive and Elastic Bottlebrush Elastomers for Ultrasoft Electronics. *Nat. Commun.* **2023**, *14*, 623.

(5) Song, J.; Huang, Y.; Xiao, J.; Wang, S.; Hwang, K. C.; Ko, H. C.; Kim, D. H.; Stoykovich, M. P.; Rogers, J. A. Mechanics of Noncoplanar Mesh Design for Stretchable Electronic Circuits. *J. Appl. Phys.* **2009**, *105*, No. 123516.

(6) Wang, Z.; Zhang, L.; Duan, S.; Jiang, H.; Shen, J.; Li, C. Kirigami-Patterned Highly Stretchable Conductors from Flexible Carbon Nanotube-Embedded Polymer Films. *J. Mater. Chem. C Mater.* **2017**, *5*, 8714−8722.

(7) Khang, D. Y.; Jiang, H.; Huang, Y.; Rogers, J. A. A Stretchable Form of Single-Crystal Silicon for High-Performance Electronics on Rubber Subtrates. *Science* **2006**, *311*, 208−212.

(8) Kim, D. H.; Ahn, J. H.; Won, M. C.; Kim, H. S.; Kim, T. H.; Song, J.; Huang, Y. Y.; Liu, Z.; Lu, C.; Rogers, J. A. Stretchable and Foldable Silicon Integrated Circuits. *Science* **2008**, *320*, 507−511.

(9) Zokaei, S.; Kim, D.; Järsvall, E.; Fenton, A. M.; Weisen, A. R.; Hultmark, S.; Nguyen, P. H.; Matheson, A. M.; Lund, A.; Kroon, R.; Chabinyc, M. L.; Gomez, E. D.; Zozoulenko, I.; Müller, C. Tuning of the Elastic Modulus of a Soft Polythiophene through Molecular Doping. *Mater. Horiz.* **2022**, *9*, 433−443.

(10) Moulton, J.; Smith, P. Electrical and Mechanical Properties of Oriented Poly(3-Alkylthiophenes) I. Doping-Enhanced Stiffness of Poly(3-Octylthiophene). *Synth. Met.* **1991**, *40*, 13−22.

(11) Kroon, R.; Hofmann, A. I.; Yu, L.; Lund, A.; Müller, C. Thermally Activated in Situ Doping Enables Solid-State Processing of Conducting Polymers. *Chem. Mater.* **2019**, *31*, 2770−2777.

(12) Hynynen, J.; Järsvall, E.; Kroon, R.; Zhang, Y.; Barlow, S.; Marder, S. R.; Kemerink, M.; Lund, A.; Müller, C. Enhanced Thermoelectric Power Factor of Tensile Drawn Poly(3-Hexylthiophene). *ACS Macro Lett.* **2019**, *8*, 70−76.

(13) Zhao, Y.; Zhao, X.; Zang, Y.; Di, C.; Diao, Y.; Mei, J. Conjugation-Break Spacers in Semiconducting Polymers: Impact on Polymer Processability and Charge Transport Properties. *Macromolecules* **2015**, *48*, 2048−2053.

(14) Wang, G.-J. N.; Molina-Lopez, F.; Zhang, H.; Xu, J.; Wu, H.-C.; Lopez, J.; Shaw, L.; Mun, J.; Zhang, Q.; Wang, S.; Ehrlich, A.; Bao, Z. Nonhalogenated Solvent Processable and Printable High-Performance Polymer Semiconductor Enabled by Isomeric Nonconjugated Flexible Linkers. *Macromolecules* **2018**, *51*, 4976−4985.

(15) Schroeder, B. C.; Chiu, Y.; Gu, X.; Zhou, Y.; Xu, J.; Lopez, J.; Lu, C.; Toney, M. F.; Bao, Z. Non-Conjugated Flexible Linkers in Semiconducting Polymers: A Pathway to Improved Processability without Compromising Device Performance. *Adv. Electron. Mater.* **2016**, *2*, No. 1600104.

(16) Xiao, W.-J.; Wang, J.; Li, H.-J.; Liang, L.; Xiang, X.; Chen, X.-Q.; Li, J.; Lu, Z.; Li, W.-S. Interconnecting Semiconducting Molecules with Non-Conjugated Soft Linkers: A Way to Improve Film Formation Quality without Sacrifice in Charge Mobility. *RSC Adv.* **2018**, *8*, 23546−23554.

(17) Savagatrup, S.; Zhao, X.; Chan, E.; Mei, J.; Lipomi, D. J. Effect of Broken Conjugation on the Stretchability of Semiconducting Polymers. *Macromol. Rapid Commun.* **2016**, *37*, 1623−1628.

(18) Shin, M.; Oh, J. Y.; Byun, K. E.; Lee, Y. J.; Kim, B.; Baik, H. K.; Park, J. J.; Jeong, U. Polythiophene Nanofibril Bundles Surface-Embedded in Elastomer: A Route to a Highly Stretchable Active Channel Layer. *Adv. Mater.* **2015**, *27*, 1255−1261.

(19) Song, E.; Kang, B.; Choi, H. H.; Sin, D. H.; Lee, H.; Lee, W. H.; Cho, K. Stretchable and Transparent Organic Semiconducting Thin Film with Conjugated Polymer Nanowires Embedded in an Elastomeric Matrix. *Adv. Electron. Mater.* **2016**, *2*, No. 1500250.

(20) Xu, J.; Wang, S.; Wang, G.-J. N.; Zhu, C.; Luo, S.; Jin, L.; Gu, X.; Chen, S.; Feig, V. R.; To, J. W. F.; Rondeau-Gagné, S.; Park, J.; Schroeder, B. C.; Lu, C.; Oh, J. Y.; Wang, Y.; Kim, Y.-H.; Yan, H.;

Sinclair, R.; Zhou, D.; Xue, G.; Murmann, B.; Linder, C.; Cai, W.; Tok, J. B.-H.; Chung, J. W.; Bao, Z. Highly Stretchable Polymer Semiconductor Films through the Nanoconfinement Effect. *Science* **2017**, *355*, 59−64.
(21) Liu, K.; Wei, S.; Song, L.; Liu, H.; Wang, T. Conductive Hydrogels - A Novel Material: Recent Advances and Future Perspectives. *J. Agric. Food Chem.* **2020**, *68*, 7269−7280.
(22) Yuk, H.; Lu, B.; Zhao, X. Hydrogel Bioelectronics. *Chem. Soc. Rev.* **2019**, *48*, 1642−1667.
(23) Danielsen, S. P. O.; Sanoja, G. E.; McCuskey, S. R.; Hammouda, B.; Bazan, G. C.; Fredrickson, G. H.; Segalman, R. A. Mixed Conductive Soft Solids by Electrostatically Driven Network Formation of a Conjugated Polyelectrolyte. *Chem. Mater.* **2018**, *30*, 1417−1426.
(24) Shin, M. K.; Oh, J.; Lima, M.; Kozlov, M. E.; Kim, S. J.; Baughman, R. H. Elastomeric Conductive Composites Based on Carbon Nanotube Forests. *Adv. Mater.* **2010**, *22*, 2663−2667.
(25) Hu, N.; Karube, Y.; Arai, M.; Watanabe, T.; Yan, C.; Li, Y.; Liu, Y.; Fukunaga, H. Investigation on Sensitivity of a Polymer/Carbon Nanotube Composite Strain Sensor. *Carbon N Y* **2010**, *48*, 680−687.
(26) Li, Z.; Le, T.; Wu, Z.; Yao, Y.; Li, L.; Tentzeris, M.; Moon, K. S.; Wong, C. P. Rational Design of a Printable, Highly Conductive Silicone-Based Electrically Conductive Adhesive for Stretchable Radio-Frequency Antennas. *Adv. Funct. Mater.* **2015**, *25*, 464−470.
(27) Fan, Y. J.; Yu, P. T.; Liang, F.; Li, X.; Li, H. Y.; Liu, L.; Cao, J. W.; Zhao, X. J.; Wang, Z. L.; Zhu, G. Highly Conductive, Stretchable, and Breathable Epidermal Electrode Based on Hierarchically Interactive Nano-Network. *Nanoscale* **2020**, *12*, 16053−16062.
(28) Choi, S.; Han, S. I.; Jung, D.; Hwang, H. J.; Lim, C.; Bae, S.; Park, O. K.; Tschabrunn, C. M.; Lee, M.; Bae, S. Y.; Yu, J. W.; Ryu, J. H.; Lee, S. W.; Park, K.; Kang, P. M.; Lee, W. B.; Nezafat, R.; Hyeon, T.; Kim, D. H. Highly Conductive, Stretchable and Biocompatible Ag−Au Core−Sheath Nanowire Composite for Wearable and Implantable Bioelectronics. *Nat. Nanotechnol.* **2018**, *13*, 1048−1056.
(29) Ma, R.; Kang, B.; Cho, S.; Choi, M.; Baik, S. Extraordinarily High Conductivity of Stretchable Fibers of Polyurethane and Silver Nanoflowers. *ACS Nano* **2015**, *9*, 10876−10886.
(30) Dauzon, E.; Lin, Y.; Faber, H.; Yengel, E.; Sallenave, X.; Plesse, C.; Goubard, F.; Amassian, A.; Anthopoulos, T. D. Stretchable and Transparent Conductive PEDOT:PSS-Based Electrodes for Organic Photovoltaics and Strain Sensors Applications. *Adv. Funct. Mater.* **2020**, *30*, No. 2001251.
(31) Lee, J. H.; Jeong, Y. R.; Lee, G.; Jin, S. W.; Lee, Y. H.; Hong, S. Y.; Park, H.; Kim, J. W.; Lee, S. S.; Ha, J. S. Highly Conductive, Stretchable, and Transparent PEDOT:PSS Electrodes Fabricated with Triblock Copolymer Additives and Acid Treatment. *ACS Appl. Mater. Interfaces* **2018**, *10*, 28027−28035.
(32) Guo, L.; Ma, M.; Zhang, N.; Langer, R.; Anderson, D. G. Stretchable Polymeric Multielectrode Array for Conformal Neural Interfacing. *Adv. Mater.* **2014**, *26*, 1427−1433.
(33) Moniruzzaman, M.; Winey, K. I. Polymer Nanocomposites Containing Carbon Nanotubes. *Macromolecules* **2006**, *39*, 5194−5205.
(34) Kim, J. H.; Hwang, J. Y.; Hwang, H. R.; Kim, H. S.; Lee, J. H.; Seo, J. W.; Shin, U. S.; Lee, S. H. Simple and Cost-Effective Method of Highly Conductive and Elastic Carbon Nanotube/Polydimethylsiloxane Composite for Wearable Electronics. *Sci. Rep.* **2018**, *8*, 1375.
(35) Yu, Z.; Niu, X.; Liu, Z.; Pei, Q. Intrinsically Stretchable Polymer Light-Emitting Devices Using Carbon Nanotube-Polymer Composite Electrodes. *Adv. Mater.* **2011**, *23*, 3989−3994.
(36) Kayser, L. V.; Lipomi, D. J. Stretchable Conductive Polymers and Composites Based on PEDOT and PEDOT:PSS. *Adv. Mater.* **2019**, *31*, No. 1806133.
(37) Self, J. L.; Reynolds, V. G.; Blankenship, J.; Mee, E.; Guo, J.; Albanese, K.; Xie, R.; Hawker, C. J.; de Alaniz, J. R.; Chabinyc, M. L.; Bates, C. M. Carbon Nanotube Composites with Bottlebrush Elastomers for Compliant Electrodes. *ACS Polymers Au* **2022**, *2*, 27−34.
(38) Wang, M.; Baek, P.; Akbarinejad, A.; Barker, D.; Travas-Sejdic, J. Conjugated Polymers and Composites for Stretchable Organic Electronics. *J. Mater. Chem. C Mater.* **2019**, *7*, 5534−5552.
(39) Natansohn, A.; Murali, R.; Eisenberg, A. Miscibility Enhancement in Polymers via Ionic Interactions: Dynamic Mechanical and NMR Studies. *Makromol. Chem. Macromol. Symp.* **1988**, *16*, 175−193.
(40) Tannenbaum, R.; Rutkowska, M.; Eisenberg, A. Ionomeric Blends. V. FTIR Studies of Ionic Interactions in Polyurethane-styrene Blends. *J. Polym. Sci., Part B: Polym. Phys.* **1987**, *25*, 663−671.
(41) Natansohn, A.; Rutkowska, M.; Eisenberg, A. Nuclear Magnetic Resonance Studies of Ionomers: 2. Proton Transfer in Polyurethane-Poly(Styrene-Co-Styrene Sulphonic Acid) Mixtures in Solution. *Polymer* **1987**, *28*, 885−888.
(42) Rutkowska, M.; Eisenberg, A. Ionomeric Blends. 3. Miscibility Enhancement via Ionic Interactions in Polyurethane-Styrene Blends. *Macromolecules* **1984**, *17*, 821−824.
(43) Natansohn, A.; Eisenberg, A. Nuclear Magnetic Resonance Studies of Ionomers. 1. Interactions between Poly(Methyl Methacrylate-Co-4-Vinylpyridine) and Poly(Styrene-Co-Styrenesulfonic Acid) in Dimethyl Sulfoxide Solution. *Macromolecules* **1987**, *20*, 323−329.
(44) Zhang, X.; Natansohn, A.; Eisenberg, A. Intermolecular Cross-Polarization Studies of The Miscibility Enhancement of PS/PMMA Blends Through Ionic Interactions. *Macromolecules* **1990**, *23*, 412−416.
(45) Noro, A.; Ishihara, K.; Matsushita, Y. Nanophase-Separated Supramolecular Assemblies of Two Functionalized Polymers via Acid-Base Complexation. *Macromolecules* **2011**, *44*, 6241−6244.
(46) Russell, T. P.; Jérôme, R.; Charlier, P.; Foucart, M. The Microstructure of Block Copolymers Formed via Ionic Interaction. *Macromolecules* **1988**, *21*, 1709−1717.
(47) Grzetic, D. J.; Delaney, K. T.; Fredrickson, G. H. Electrostatic Manipulation of Phase Behavior in Immiscible Charged Polymer Blends. *Macromolecules* **2021**, *54*, 2604−2616.
(48) Fredrickson, G. H.; Xie, S.; Edmund, J.; Le, M. L.; Sun, D.; Grzetic, D. J.; Vigil, D. L.; Delaney, K. T.; Chabinyc, M. L.; Segalman, R. A. Ionic Compatibilization of Polymers. *ACS Polymers Au* **2022**, *2*, 299−312.
(49) Le, M. L.; Rawlings, D.; Danielsen, S. P. O.; Kennard, R. M.; Chabinyc, M. L.; Segalman, R. A. Aqueous Formulation of Concentrated Semiconductive Fluid Using Polyelectrolyte Coacervation. *ACS Macro Lett.* **2021**, *10*, 1008−1014.
(50) Le, M. L.; Grzetic, D. J.; Delaney, K. T.; Yang, K. C.; Xie, S.; Fredrickson, G. H.; Chabinyc, M. L.; Segalman, R. A. Electrostatic Interactions Control the Nanostructure of Conjugated Polyelectrolyte-Polymeric Ionic Liquid Blends. *Macromolecules* **2022**, *55*, 8321−8331.
(51) Le, M. L.; Warner, C.; Segalman, R. A.; Chabinyc, M. L. Role of Complexation Strength on the Photophysical and Transport Properties of Semiconducting Charged Polymer Complexes. *Chem. Mater.* **2023**, *35*, 4449−4460.
(52) Xie, R.; Lapkriengkri, I.; Pramanik, N. B.; Mukherjee, S.; Blankenship, J. R.; Albanese, K.; Wang, H.; Chabinyc, M. L.; Bates, C. M. Hydrogen-Bonding Bottlebrush Networks: Self-Healing Materials from Super-Soft to Stiff. *Macromolecules* **2022**, *55*, 10513−10521.
(53) Kazemiabnavi, S.; Zhang, Z.; Thornton, K.; Banerjee, S. Electrochemical Stability Window of Imidazolium-Based Ionic Liquids as Electrolytes for Lithium Batteries. *J. Phys. Chem. B* **2016**, *120*, 5691−5702.
(54) Rubinstein, M.; Liao, Q.; Panyukov, S. Structure of Liquid Coacervates Formed by Oppositely Charged Polyelectrolytes. *Macromolecules* **2018**, *51*, 9572−9588.
(55) Chremos, A.; Douglas, J. F. A Comparative Study of Thermodynamic, Conformational, and Structural Properties of Bottlebrush with Star and Ring Polymer Melts. *J. Chem. Phys.* **2018**, *149*, No. 044904.
(56) Schmode, P.; Ohayon, D.; Reichstein, P. M.; Savva, A.; Inal, S.; Thelakkat, M. High-Performance Organic Electrochemical Transistors


https://doi.org/10.1021/acs.chemmater.3c01685
*Chem. Mater.* 2023, 35, 7301−7310

Based on Conjugated Polyelectrolyte Copolymers. *Chem. Mater.* **2019**, *31*, 5286−5295.
(57) Paquin, F.; Yamagata, H.; Hestand, N. J.; Sakowicz, M.; Bérubé, N.; Côté, M.; Reynolds, L. X.; Haque, S. A.; Stingelin, N.; Spano, F. C.; Silva, C. Two-Dimensional Spatial Coherence of Excitons in Semicrystalline Polymeric Semiconductors: Effect of Molecular Weight. *Phys. Rev. B Condens. Matter Mater. Phys.* **2013**, *88*, No. 155202.
(58) De Jesus, M. C.; Fu, Y.; Weiss, R. A. Conductive Polymer Blends Prepared by in Situ Polymerization of Pyrrole: A Review. *Polym. Eng. Sci.* **1997**, *37*, 1936−1943.
(59) Njuguna, J.; Pielichowski, K. Recent Developments in Polyurethane-Based Conducting Composites. *J. Mater. Sci.* **2004**, *39*, 4081−4094.
(60) Zallen, R. *The Physics of Amorphous Solids*; Wiley, 1998.
(61) Suzuki, Y. Y.; Heeger, A. J.; Pincus, P. Percolation of Conducting Polymers on a Gel. *Macromolecules* **1990**, *23*, 4730.
(62) Hotta, S.; Rughooputh, S. D. D. V.; Heeger, A. J. Conducting Polymer Composites of Soluble Polythiophenes in Polystyrene. *Synth. Met.* **1987**, *22*, 79−87.
(63) Reynolds, V. G.; Mukherjee, S.; Xie, R.; Levi, A. E.; Atassi, A.; Uchiyama, T.; Wang, H.; Chabinyc, M. L.; Bates, C. M. Super-Soft Solvent-Free Bottlebrush Elastomers for Touch Sensing. *Mater. Horiz.* **2020**, *7*, 181−187.
(64) Vatankhah-Varnoosfaderani, M.; Daniel, W. F. M.; Zhushma, A. P.; Li, Q.; Morgan, B. J.; Matyjaszewski, K.; Armstrong, D. P.; Spontak, R. J.; Dobrynin, A. V.; Sheiko, S. S. Bottlebrush Elastomers: A New Platform for Freestanding Electroactuation. *Adv. Mater.* **2017**, *29*, No. 1604209.
(65) Rubinstein, M.; Colby, R. H. *Polymer Physics*; Oxford University Press, 2003.
(66) Boschin, A.; Johansson, P. Characterization of NaX (X: TFSI, FSI) − PEO Based Solid Polymer Electrolytes for Sodium Batteries. *Electrochim. Acta* **2015**, *175*, 124−133.
(67) Dong, H.; Du, H.; Wickramasinghe, S. R.; Qian, X. The Effects of Chemical Substitution and Polymerization on the PK a Values of Sulfonic Acids. *J. Phys. Chem. B* **2009**, *113*, 14094−14101.
(68) Self, J. L.; Dolinski, N. D.; Zayas, M. S.; Read de Alaniz, J.; Bates, C. M. Brønsted-Acid-Catalyzed Exchange in Polyester Dynamic Covalent Networks. *ACS Macro Lett.* **2018**, *7*, 817−821.
(69) Li, P.; Sun, K.; Ouyang, J. Stretchable and Conductive Polymer Films Prepared by Solution Blending. *ACS Appl. Mater. Interfaces* **2015**, *7*, 18415−18423.
(70) Choi, D.; Kim, H.; Persson, N.; Chu, P. H.; Chang, M.; Kang, J. H.; Graham, S.; Reichmanis, E. Elastomer-Polymer Semiconductor Blends for High-Performance Stretchable Charge Transport Networks. *Chem. Mater.* **2016**, *28*, 1196−1204.
(71) Matson, J. B.; Grubbs, R. H. Synthesis of Fluorine-18 Functionalized Nanoparticles for Use as in Vivo Molecular Imaging Agents. *J. Am. Chem. Soc.* **2008**, *130*, 6731−6733.
(72) Atzrodt, J.; Derdau, V.; Kerr, W. J.; Reid, M. Deuterium- and Tritium-Labelled Compounds: Applications in the Life Sciences. *Angew. Chem. Int. Ed.* **2018**, *57*, 1758−1784.
(73) Levi, A. E.; Lequieu, J.; Horne, J. D.; Bates, M. W.; Ren, J. M.; Delaney, K. T.; Fredrickson, G. H.; Bates, C. M. Miktoarm Stars via Grafting-Through Copolymerization: Self-Assembly and the Star-to-Bottlebrush Transition. *Macromolecules* **2019**, *52*, 1794−1802.
(74) Levi, A. E.; Fu, L.; Lequieu, J.; Horne, J. D.; Blankenship, J.; Mukherjee, S.; Zhang, T.; Fredrickson, G. H.; Gutekunst, W. R.; Bates, C. M. Efficient Synthesis of Asymmetric Miktoarm Star Polymers. *Macromolecules* **2020**, *53*, 702−710.


https://doi.org/10.1021/acs.chemmater.3c01685
*Chem. Mater.* 2023, 35, 7301−7310